

# Theoretical and experimental results of a mesoscale electric power generation system from pressurized gas flow

D Krähenbühl<sup>1</sup>, C Zwysig<sup>2</sup>, H Weser<sup>3</sup> and J W Kolar<sup>1</sup>

<sup>1</sup> Power Electronic System Laboratory, ETH Zurich, Switzerland

<sup>2</sup> Celeroton Ltd, Zurich, Switzerland

<sup>3</sup> High Speed Turbomaschinen GmbH, Wolfsburg, Germany

Received 16 December 2008, in final form 27 May 2009

Published 26 August 2009

Online at [stacks.iop.org/JMM/19/094009](http://stacks.iop.org/JMM/19/094009)

## Abstract

In many process applications where throttling is used to reduce pressure, the potential to obtain net work output is sacrificed to the throttling process. Examples are throttling valves of gas pipelines and conventional throttles in automotive applications or turbo expanders as used in cryogenic plants. With a new pressure reduction system that produces electricity while expanding the gas, the lost potential to obtain work output can be recovered. To achieve a high power density, this energy generation system requires an increased operating speed of the electrical machine and the turbomachinery. This paper presents a miniature compressed-air-to-electric-power system, based on a radial turbine with a rated rotational speed of 490 000 rpm and a rated electric power output of 150 W. A comprehensive description including turbine, diffuser and permanent magnet (PM) generator is given. Finally, measurements of the compressed-air-to-electric-power system with a maximum rotational speed of over 600 000 rpm, a maximum electric output power of 170 W, a maximum torque of 5.2 mN m and a turbine efficiency of 52% are presented.

(Some figures in this article are in colour only in the electronic version)

## Introduction

In pressure reduction devices, such as valves, conventional throttles or turbo expanders, the ability to obtain work from the pressure drop is usually sacrificed. However, this potential work could be recovered by employing a system that removes energy from the pressurized gas flow and converts it into electrical energy.

One example is the replacement of the conventional throttle in automotive applications where a turbine in combination with a generator can actively throttle the intake air and thereby produce electrical power [1]. Measurements at constant speed have shown that up to 700 W of electric power could be extracted (turbine  $\varnothing$ 40 mm) and an extrapolation with a 50% downsized turbine predicts that even more electric power could be produced.

While it is necessary to transport natural gas at high pressures, end-users require gas delivery at only a fraction of the main pipeline pressure. Therefore, energy can be

recovered at pressure reduction stations if throttling valves are replaced by expanders driving electrical generators [2]. For power recovery, turbines are generally rated from 150 kW to 2.5 MW; however, the pressure reduction process is usually done in several stages, and an array of small turbine-generator modules could replace one large pressure reduction valve [2].

In cryogenic plants, output stage turbo expanders (in the kW range) are braked through a compressor. The compressed and the hot fluid is cooled with a water cooler and expanded over a brake valve. The three components compressor, cooler and valve could be replaced with a single generator and thereby produce electricity. Hence, the efficiency of such plants could be increased [4]. Since the turbo expander and the brake cooler are located near each other, the temperature gradient between the cool expander and the warm compressor is extremely high. With the use of an electrical break no such high temperature gradient would occur, which is a further advantage.

Several of the above-mentioned applications, e.g. in automobiles, require ultra-compact systems. Power density in

both turbomachinery and electrical machines increases with increasing rotational speed [5, 6]. Therefore, for highest power density, these systems are operating at rotational speeds between 100 000 rpm and 1 Mrpm at power levels of up to several kilowatts.

## Research landscape

Besides common high power gas turbines for centralized power generation, micro-turbines with less than 100 W power output and very high rotational speeds have been reported in the literature, usually for distributed and/or portable power generation.

In [7], a modular system consisting of an off-the-shelf air turbine from a dental drill, a permanent-magnet (PM) generator and a rectifier has been realized, with a maximum power output of 1.11 W and a maximum speed of 200 000 rpm. Drawbacks of this system are the poor power density ( $0.02 \text{ W cm}^{-3}$ ) and the large inlet flow rate of  $45 \text{ l min}^{-1}$  at maximum output power. The power electronics of the system consist of a three-phase transformer, a diode bridge rectifier and a 5 V linear regulator.

In [8], a single-stage axial turbine coupled to a commercial electrical machine with a maximum electric power output of 16 W at 160 000 rpm and 100 kPa supply pressure has been introduced for later use in a gas turbine system. The maximum torque and mechanical power generated from the turbine is 3.7 mN m and 28 W, respectively. The generator is connected to a variable three-phase resistive load to measure the electric output power. The total system has a maximum efficiency of 10.5% at 100 000 rpm and achieves a power density of  $1.6 \text{ W cm}^{-3}$ , excluding power and control electronics.

In [9], a PM generator, capable of supplying 8 W of dc power to a resistive load at a rotational speed of 305 000 rpm, is presented. The stator uses interleaved, electroplated copper windings on a magnetically soft substrate. The rotor consists of an 8-pole SmCo PM, a back iron and a titanium sleeve to limit the centrifugal forces on the PM. The machine was characterized using an air-driven spindle. To provide a dc voltage, the ac generator voltages were first stepped up using a three-phase transformer and then converted to dc using a three-phase Schottky diode rectifier. The dimensions of the device are chosen with reference to a future integration into a micro turbine engine. This leads to a power density of the generator of  $59 \text{ W cm}^{-3}$  and to a generator efficiency of 28%. The combination of [9] with a silicon turbine is presented in [10]. The generator of this fully integrated permanent-magnet turbine generator device has delivered 19 mW to a resistive load at a rotational speed of 40 000 rpm.

A planar generator with a diameter of 8 mm consisting of a permanent magnet disc rotor cut out of bulk SmCo or NdFeB protected by a titanium sleeve, and a silicon stator with electroplated three-phase planar coils is presented in [11]. The generator is driven by a planar turbine, etched into the opposite side of the rotor. Due to the turbine construction, the speed is limited to 100 000 rpm with 500 kPa compressed air supply. A maximum power output of 14.6 mW was measured at 58 000 rpm with three Y-connected  $50 \Omega$  resistors. Using

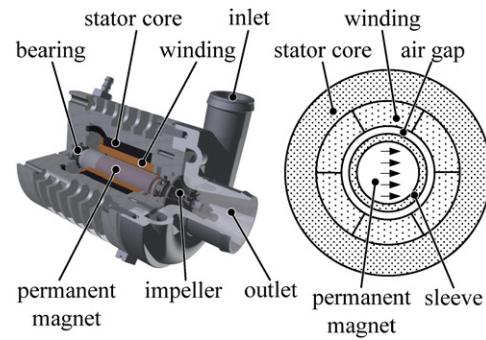


**Figure 1.** Solid model and machine cross-section of the compressed-air-to-electric power generation system: diametrically magnetized cylindrical permanent magnet rotor inside a slotless stator. Outer dimensions:  $33 \times 43 \text{ mm}$ .



**Figure 2.** PM generator with stator guide vanes, spiral casing and radial turbine ( $d = 10.5 \text{ mm}$ ).

a turbine of a dental drill, the rotor reached a maximum speed of 420 000 rpm. With this setup, the highest electric power output of 5 W (three Y-connected  $12 \Omega$  resistors) was reached at 380 000 rpm with an electrical efficiency of 66%.

In [12], an ultra-compact and fully integrated compressed-air-to-electric-power system with a rated rotational speed of 350 000 rpm and a rated power output of 60 W is presented. This compressed-air-to-electric-power system comprises a single-stage axial impulse turbine (Laval turbine) and a PM generator. Before the pressurized inlet air reaches the nozzle guide vanes and the impulse turbine, it is first diverted into eight channels that are arranged symmetrically around the generator. This leads to higher effort in the construction of the casing, but the generator and the ball bearings can be cooled. Measurements show that the system has a maximum power output of 124 W at 370 000 rpm and 600 kPa supply pressure and a maximum system efficiency (turbine and generator) of 24% at 350 000 rpm. The integrated system has a total volume of  $22.8 \text{ cm}^3$  ( $d = 2.2 \text{ cm}$ ,  $l = 6 \text{ cm}$ ) which leads to a generator and turbine power density of  $5.4 \text{ W cm}^{-3}$ .

In this paper, the theoretical and experimental results of a mesoscale compressed-air-to-electric power generation system are presented (figures 1 and 2).

## System description

The compressed-air-to-electric-power system (figures 1 and 2) under investigation has a rated rotational speed of 490 000 rpm and a rated power output of 150 W. It is based on the

**Table 1.** Electrical data

Rated speed $n_r$	490 000 rpm
Rated electric output $P_{el}$	150 W
Magnet flux linkage $\Psi_{PM}$	0.22 mVs
Back EMF at rated speed	11.2 V
Stator inductance $L_S$	2.25 $\mu$ H
Stator resistance $R_S$	0.125 $\Omega$
Machine efficiency $\eta_{mr}$	87%

reversal of an existing electric motor-driven compressor system [13], which reaches a maximum pressure ratio of 1.6 at a maximum rotational speed of 550 000 rpm with a power input of 150 W. Possible applications for electrically driven compressors are fuel cells, heat pumps, aerospace and automotive air pressurization, heating, ventilation and air conditioning systems. Power levels of these compressors are ranging from 100 W up to a few kilowatts.

Replacing the vane-less compressor diffuser with new and specially designed guide vanes, the motor-driven compressor system can be reversed and operated as a turbine-generator system. The original compressor is thereby running backwards as a turbine. This new compressed-air-to-electric-power system comprises an inward-flow radial (IFR) turbine and a PM generator. The PM generator and turbine have a total volume of 36.8 cm<sup>3</sup> ( $d = 3.3$  cm,  $l = 4.3$  cm), which leads to a power density of 4 W cm<sup>-3</sup>.

For the existing turbo compressor system, a detailed electromagnetic machine design, an analysis of the mechanical stresses and rotor dynamics and a thermal design have already been made. These design considerations are also valid for the compressed-air-to-electric-power system, and only the thermodynamic design and the guide vanes have to be modified.

### Electrical considerations

The rotor of the PM generator consists of a diametrically magnetized cylindrical SmCo permanent magnet ( $l = 15$  mm,  $d = 4.9$  mm) encased in a retaining titanium sleeve ensuring sufficiently low mechanical stresses on the magnet. The eccentricity is minimized by shrink fitting the sleeve onto the permanent magnet and grinding the rotor. The PM generator utilizes two high-speed ball bearings due to its simplicity and small size (inner diameter: 3.175 mm, outer diameter: 6.35 mm,  $l = 2.8$  mm). The stator magnetic field rotates with high frequency (8.3 kHz); it is therefore necessary to minimize the losses in the stator core by using amorphous iron. In order to minimize the eddy current losses in the copper wires, the three-phase air-gap winding is realized with litz wire. Considering the magnet flux linkage  $\Psi_{PM}$ , the motor has a peak phase-to-phase voltage of 19.4 V at 490 000 rpm. The length of the shaft is adjusted such that rated speed falls in between the second and the third bending mode. The measured electrical machine efficiency  $\eta_{mr}$  at rated power output is 87% including air friction and bearing losses. A detailed description of the generator has been presented in [13], and in table 1 the rated and measured electrical data of the PM motor is summarized.

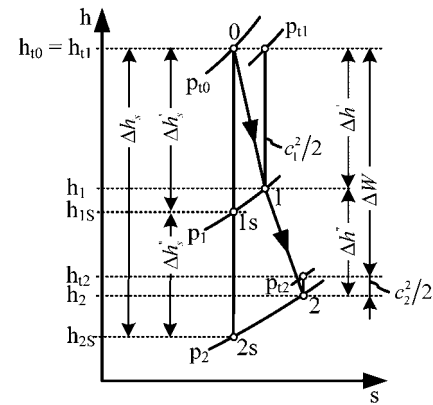


**Figure 3.** Enthalpy entropy diagram (hs-diagram) specific work:  $\Delta W = u_1 c_{u1} - u_2 c_{u2}$ .

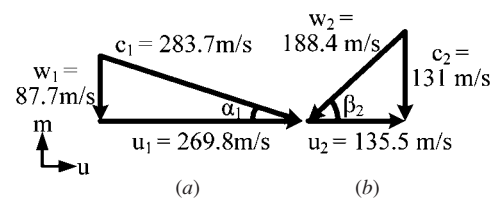


**Figure 4.** Velocity diagrams at rotor entry (a) and outlet (b) for the rated rotational speed.  $c_1/c_2$  absolute velocity at rotor inlet/outlet.  $w_1/w_2$  relative velocity at rotor inlet/outlet.  $u_1/u_2$  stator speed at radius  $r_3$  and  $\bar{r}_{4,5}$ .

### Turbomachinery considerations

The system was originally designed as an electrically driven compressor. Therefore, the dimensions of the impeller are given, especially the inlet and outlet angle of the rotor blades. For this reason, the stator guide vanes have to be adjusted to meet optimum efficiency at a rated rotational speed of 490 000 rpm. Since the inlet angle of the turbine blade is zero, the relative velocity  $w_1$  has to be orthogonal to the rotational speed  $u_1$  (figure 4(a)).

The complete adiabatic expansion process for a turbine is represented by the enthalpy–entropy diagram (Mollier diagram), shown in figure 3. The ideal enthalpy change ( $\Delta h_s$ ), i.e. the ideal or reversible expansion, is in between the inlet and outlet pressure, but at constant entropy (line 0–1s–2s). Assuming adiabatic flow through the turbine, the corresponding temperature drop  $\Delta T_{(0-2s)}$  can be calculated as

$$\Delta T_{(0-2s)} = T_0 \left( 1 - \frac{p_{t0}^{\left(\frac{1-\kappa}{\kappa}\right)}}{p_2} \right) = 83.4 \text{ K} \quad (1)$$

where  $\kappa$  is the specific heat ratio. The actual expansion follows the line 0–1–2. The temperature drop  $\Delta T_2$  can be calculated with the assumed isentropic efficiency  $\eta_{is}$ , which can be estimated from correlations of experimental data and is supposed to be 70%:

$$\Delta T_2 = \Delta T_{(0-2s)} \eta_{is} = 58.4 \text{ K} \rightarrow T_2 = 241.6 \text{ K}. \quad (2)$$

In an adiabatic turbomachine, the flow work determines the change of enthalpy. The losses (dissipation work) are uniquely caused by the increase in entropy of the fluid.

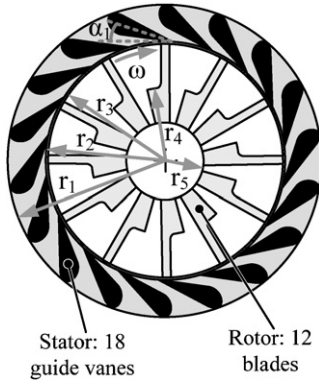


**Figure 5.** Radial turbine ( $r_1$ : 7 mm,  $r_2$ : 5.335 mm,  $r_3$ : 5.25 mm,  $r_4$ : 3.3 mm,  $r_5$ : 1.75 mm,  $\alpha_1$ : 18°).

The temperature  $T_1$  in between the stator and rotor can be calculated via the specific kinetic energy of the absolute velocity at rotor entry  $c_1$ :

$$\Delta T_{(0-1s)} = \frac{\Delta h'}{c_p \eta_n} = \frac{c_1^2}{2c_p \eta_n} = 44.5 \text{ K} \quad (3)$$

$$\Delta T_{(0-1)} = \frac{\Delta h'}{c_p} = \Delta T_{(0-1s)} \eta_n = \frac{c_1^2}{2c_p} = 40.1 \text{ K} \quad (4)$$

where  $c_p$  is the specific heat capacity. As a result of miniaturization, and therefore a larger influence of side friction, the guide vane efficiency  $\eta_n$  was assumed to be 90%.

The pressure  $p_1$  in between the stator and rotor can now be calculated as

$$p_1 = p_{t0} \left( 1 - \frac{\Delta T_{(0-1s)}}{T_0} \right)^{\frac{\kappa}{\kappa-1}} = 200 \text{ kPa}. \quad (5)$$

In figure 5, the layout of the stator and the rotor is plotted. From the rotor inlet ( $r_3$ ), the rotor blades extend radially inward and turn the flow into the axial direction. The exit part of the blades is curved to remove the absolute tangential component of velocity. In figure 4(b), the velocity diagram for the turbine outlet is drawn. The air gap between the radial turbine and the spiral casing has to be as thin as possible, in order to minimize the tip leakage losses. The constant mass flow rate through the turbine can be written as

$$\dot{m} = \rho_1 c_{m1} A_{u1} = \left( \frac{p_1}{RT_1} \right) w_1 A_{u1} = 4 \text{ g s}^{-1} \quad (6)$$

where  $R$  is the ideal gas constant. The effective turbine inlet area  $A_1$  also accounts for the rotor blade thickness. The maximum output power of the turbine can now be calculated as

$$P = \dot{m} \cdot 1/2[(c_1^2 - c_2^2) + (u_1^2 - u_2^2) + (w_2^2 - w_1^2)] \\ = \dot{m} \cdot (u_1 c_{u1} - u_2 c_{u2}) = \dot{m} \cdot u_1^2 = 291 \text{ W} \quad (7)$$

where  $c_{u1} = u_1$  and  $c_{u2} = 0 \text{ m s}^{-1}$ . From this value, the leakage losses, the tip clearance losses and the side friction of the turbine disc back are deducted. In table 2, the calculated thermodynamic and turbine data are summarized.

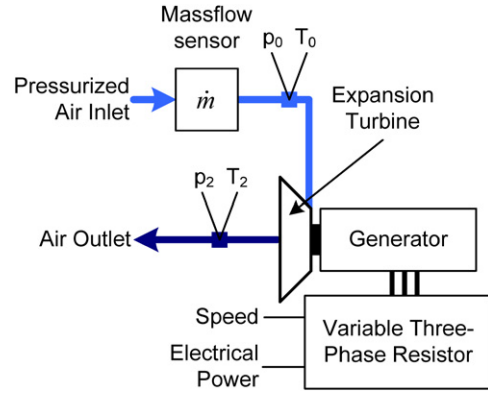


**Figure 6.** Test bench setup.

**Table 2.** Thermodynamic and turbine data.

Inlet temperature $T_0$	300 K
Inlet pressure $p_{t0}$	350 kPa
Outlet pressure $p_2$	112 kPa
Guide vane efficiency $\eta_n$	90%
Isentropic efficiency $\eta_{is}$	70%
Effective turbine inlet area $A_{u1}$	17 mm <sup>2</sup>
Effective turbine exit area $A_{u2}$	19.5 mm <sup>2</sup>

### Test bench setup

In order to verify theoretical considerations and the compressed-air-to-power system concept, an experimental test bench, shown in figure 6, has been built. It includes a mass flow sensor and several temperature and pressure sensors and a three-phase variable resistive load. The system has been tested up to an inlet pressure of 300 kPa and a maximum outlet electric power of 170 W. For the measurements, the operating point could be changed by varying the resistive three-phase load and the supply pressure. In addition to input and output pressure, the input and output temperature of the air flow have been measured. As expected, the efficiency could not be measured depending on the temperature drop because the turbine is not isolated enough from the thermal losses of the generator and ball bearings. The turbine and generator speed can be determined from the current in the resistive load. Similarly, with a three-phase power analyser, the electric output power can be measured.

Assuming adiabatic flow through the turbine, the pressurized-air-to-electric-power efficiency has been calculated using

$$\eta_{\text{system}} = \frac{P_{\text{el}}}{\dot{m} \cdot \Delta T_{(0-2s)} \cdot c_p} \quad (8)$$

where  $c_p$  is the specific heat capacity,  $P_{\text{el}}$  is the electric output power and  $\Delta T_{(0-2s)}$  is taken from (1). With the knowledge of the generator efficiency, the turbine efficiency (product of isentropic efficiency and volumetric efficiency) can now be calculated as

$$\eta_{\text{turbine}} = \eta_{is} \cdot \eta_v = \frac{\eta_{\text{system}}}{\eta_{\text{generator}}} \quad (9)$$

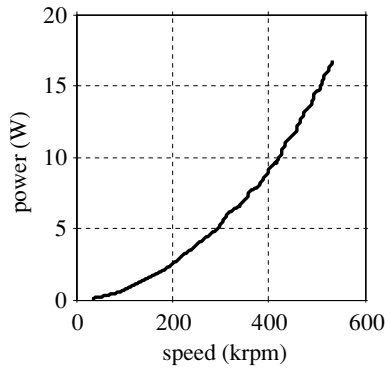


**Figure 7.** Measured losses of the high-speed motor versus speed. The measured power losses include bearing losses, windage losses and core losses. For the total generator losses, the calculated copper losses are added.

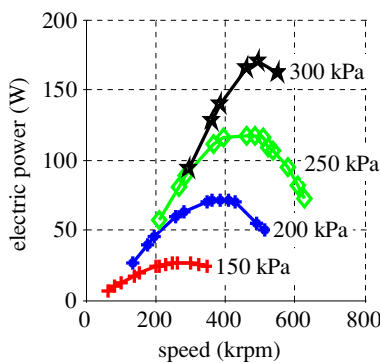


**Figure 8.** Electrical power generated by the turbine and generator system as a function of speed and supply pressure.

The generator efficiency is determined from the measured losses shown in figure 7 plus the calculated copper losses.

### Measurements

First, the motor has been tested without load up to a maximum speed of 550 000 rpm, and the bearing, windage and core losses were measured with a deceleration test (figure 7). Not included in the deceleration test are the copper losses depending on the phase currents, but they can be calculated accurately with the measured phase resistance  $R_s$  (table 1) and added to the measured generator losses.

In the second step, the impeller and inlet housing are mounted. Figures 8 and 9 show the electric output power and torque as a function of speed and supply pressure. The maximum electric power output is around 170 W at 495 000 rpm, and the maximum measured torque is 5.2 mNm at 295 000 rpm. An increase in the three-phase resistance causes a decrease in the torque and therefore an increasing speed at a constant supply pressure.

Figure 10 shows the turbine efficiency as a function of speed and supply pressure. The maximum turbine efficiency is around 52%, while the maximum system efficiency (turbine and generator) is 43%.

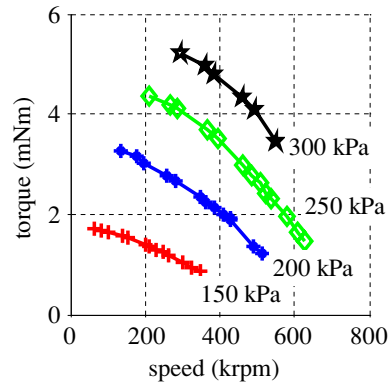


**Figure 9.** Torque generated by the turbine as a function of speed and supply pressure.

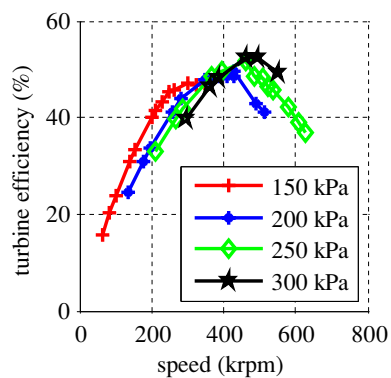


**Figure 10.** Turbine efficiency as a function of speed and inlet pressure.

### Comparison

Comparing radial turbines with axial impulse turbines such as in [8] and [12], the turbine efficiency (52% versus 18% and 28% respectively) and the system efficiency (43% versus 10.5% and 24% respectively) are higher for the radial turbine. This is because radial turbines generally have higher efficiency than radial impulse turbines, but the manufacturing and the controlling of tolerances are more difficult. The maximum generator efficiency (83%) is significantly higher compared to the generator presented in [9] (28%).

In [9] and [11], the  $\mu$ -generators are driven with simple air-driven turbines and therefore only the generator power density is presented. Therefore, comparing the generator power densities of the different systems, it can be seen that the traditionally fabricated systems, as in [12], and the system presented in this paper have power densities in the same range ( $11 \text{ W cm}^{-3}$  versus  $6 \text{ W cm}^{-3}$ ), while systems that have electroplated surface windings and are made using deep lithography or silicon etching, as in [9–11], have power densities up to  $59 \text{ W cm}^{-3}$ . On the other hand, the maximum electric output is clearly higher with traditionally fabricated systems ( $124 \text{ W}$  and  $170 \text{ W}$  versus  $5 \text{ W}$  and  $8 \text{ W}$ ). Also the generator efficiencies of [9] and [11] (28% and 66%) are much lower than that in the high-speed generator used in the system presented in this paper (83%).

## Conclusion

This paper has investigated an existing eclectically driven high-speed radial compressor system that is reversed to a compressed-air-to-power system. To the authors' knowledge, it is the first experimentally validated turbine-generator system with a speed exceeding 600 000 rpm and an output power exceeding 100 W. Measurements show that the system has a maximum power output of 170 W at 495 000 rpm and a maximum efficiency of 52%. Compared to other systems published in the literature such as in [9–12], the compressed-air-to-electric-power system presented has a significantly higher electric output power and a higher system efficiency.

The reasons for the higher system efficiency are the use of self-optimized, matched and produced components. During assembly, special attention to the impeller–stator tip clearance has been given. Keeping this air gap as small as possible has a significant influence on the overall efficiency. In order to reach small tip clearances, the rotor–impeller assembly requires advanced balancing technology. Also, the compressor blade thickness has been chosen to be as thin as possible, in order not to reduce the inlet and outlet area.

The generator has been optimized for lowest losses. For this reason, an optimization method has been developed which takes air friction losses, iron losses, copper losses and eddy current losses into account. The optimization results show that air friction losses influence the optimum design considerably, leading to a small rotor diameter at high speeds.

The system described in this paper has a rather small output power level for the applications listed in the introduction, but it is scalable, especially with a modular approach with several small systems replacing one big system. Concerning power density and efficiency, the system is very attractive.

However, bearing lifetime is the main challenge before such ultra-high-speed turbine generator systems (or electrically driven compressors) can get widely used in industry. For reaching the acceptable lifetime the high-speed

ball bearings must get replaced by air bearings or magnetic bearings.

## References

- [1] Guzzella L, Betschart M, Fluri T, De Santis R, Onder C and Auckenthaler T 2004 Recuperative throttling of SI engines for improved fuel economy *SAE 2004 World Congress & Exhibition*
- [2] Mirandola A and Minca L 1986 Energy recovery by expansion of high pressure natural gas *Proc. 21st Intersociety Energy Conversion Engineering Conf.* vol 1 pp 16–21
- [3] Lehman B and Worrell E 2001 Electricity production from natural gas pressure recovery using expansion turbines *ACEEE* **2** 43–54
- [4] LeGoy P R 1999 Utility requirements for power recovery in the cryogenic and chemical industry using variable frequency drives in the regenerative mode *IEEE Power Engineering Society Summer Meeting* pp 542–6
- [5] Binder A and Schneider T 2007 High-speed inverter-fed AC drives *ACEMP* pp 9–16
- [6] Kang S, Lee S J and Prinz F B 2001 Size does matter, the pros and cons of miniaturization *ABB Rev.* **2** 54–62
- [7] Arnold D P, Galle P, Herrault F, Das S, Lang J H and Allen M G 2005 A self-contained, flow-powered microgenerator system *PowerMEMS* pp 113–5
- [8] Peirs J, Reynaerts D and Verplaetsen F 2004 A microturbine for electric power generation *Sensors Actuators* **113** 86–93
- [9] Arnold D P, Herrault F, Zana I, Galle P, Park J W, Das S, Lang J H and Allen M G 2006 Design optimization of an 8-watt, microscale, axial-flux, permanent-magnet generator *J. Micromech. Microeng.* **16** 290–6
- [10] Yen C B *et al* 2008 Characterization of a fully-integrated permanent-magnet turbine generator *PowerMEMS* pp 121–4
- [11] Raisigel H, Cugat O and Delamare J 2006 Permanent magnet planar micro-generators *Sensors Actuators* **130–131** 438–44
- [12] Krähenbühl D, Zwyssig C, Hörler H and Kolar J W 2008 Design considerations and experimental results of a 60 W compressed-air-to-electric-power system *MESA* pp 375–80
- [13] Zwyssig C, Krähenbühl D, Weser H and Kolar J W 2008 A miniature turbocompressor system *Proc. of Smart Energy Strategies (Zurich)* pp 144–9
- [14] Zwyssig C and Kolar J W 2006 Design considerations and experimental results of a 100 W, 500 000 rpm electrical generator *J. Micromech. Microeng.* **9** 297–302